

## Article

# Development of Sustainable Radiation-Shielding Blend Using Natural Rubber/NBR, and Bismuth Filler

Ola Aziz <sup>1</sup>, E. Salama <sup>2,\*</sup> , Doaa E. El-Nashar <sup>3</sup>  and Assem Bakry <sup>1</sup>

<sup>1</sup> Physics Department, Faculty of Science, Ain Shams University, Cairo 11566, Egypt; olaziz\_p@sci.asu.edu.eg (O.A.); assem.sedfy@sci.asu.edu.eg (A.B.)

<sup>2</sup> Basic Science Department, Faculty of Engineering, The British University in Egypt-BUE, El Sherouk City 11837, Egypt

<sup>3</sup> Department of Polymers and Pigments, National Research Centre, Giza 12622, Egypt; doaaelnashar@yahoo.com

\* Correspondence: elsayed.salama@bue.edu.eg; Tel.: +20-1223870849; Fax: +20-2-24665630

**Abstract:** This research entailed the production of composite materials through the combination of natural rubber and acrylonitrile butadiene rubber, along with nano-silica-loaded bismuth (III) oxide, in varying concentrations ranging from 0 to 45 parts per hundred parts of rubber (phr). The gamma attenuation properties of the composites at different concentrations of Bi<sub>2</sub>O<sub>3</sub> were measured. Additionally, the mechanical properties of the resulting composites, including hardness, tensile strength, and elongation, were tested. The composites with a concentration of 20 phr exhibited the highest tensile strength and elongation at break, followed by a subsequent decrease as the concentration of Bi<sub>2</sub>O<sub>3</sub> increased. The gamma mass-attenuation coefficient of the composites increased as the Bi<sub>2</sub>O<sub>3</sub> concentration increased from 0 to 45 phr, with values ranging from 0.083 to 0.090 cm<sup>2</sup>/g at 0.662 MeV. Moreover, the fast neutron mass removal cross-sections ranged from 0.092 to 0.072 cm<sup>2</sup>/g, corresponding to the variation of Bi<sub>2</sub>O<sub>3</sub> concentration from 0–45 phr are also determined. Various parameters related to gamma-ray shielding, including the half-value layer, exposure build-up factor (EBF) up to 40 mean free path (mfp) penetration depth, and effective atomic number ( $Z_{\text{eff}}$ ) are also included. The radiation-induced aging of the prepared blend is tested by measuring the effect of radiation exposure on its shielding capability via its porosity change. The obtained results indicated that the prepared composites could be used for several radiation-protection applications.

**Keywords:** NBR; natural rubber; bismuth; gamma shielding; buildup factor; neutron removal cross-section



check for updates

**Citation:** Aziz, O.; Salama, E.; E.

El-Nashar, D.; Bakry, A.

Development of Sustainable

Radiation-Shielding Blend Using

Natural Rubber/NBR, and Bismuth

Filler. *Sustainability* **2023**, *15*, 9679.

<https://doi.org/10.3390/su15129679>

Academic Editor: Changhyun Roh

Received: 12 April 2023

Revised: 9 June 2023

Accepted: 12 June 2023

Published: 16 June 2023



**Copyright:** © 2023 by the authors.

Licensee MDPI, Basel, Switzerland.

This article is an open access article

distributed under the terms and

conditions of the Creative Commons

Attribution (CC BY) license ([https://creativecommons.org/licenses/by/](https://creativecommons.org/licenses/by/4.0/)

[https://creativecommons.org/licenses/by/](https://creativecommons.org/licenses/by/4.0/)

4.0/).

## 1. Introduction

Nuclear radiation has various useful applications in different fields such as industries, agriculture, food irradiation, defects detection in metal casting, nuclear reactors, medical diagnostic, imaging and therapy, nuclear power plants, aerospace, and radiation chemistry of polymers [1]. Nevertheless, exposure to ionizing radiation can result in radiation sickness, organ damage, cell mutation, cancer, component failure, and other negative effects, depending on the amount of radiation absorbed. Therefore, it is essential to use shielding to protect individuals from these harmful effects.

Radiation shielding is essential for protecting people and equipment from the harmful effects of ionizing radiation. Ionizing radiation can cause damage to living tissue and DNA, leading to an increased risk of cancer, radiation sickness, and other health problems. It can also damage electronic equipment and sensitive instruments, causing malfunctions or complete failure [2]. Radiation shielding works by absorbing or scattering the radiation, reducing its intensity and protecting the people and equipment behind the shield. Shielding materials can vary depending on the type and energy of the radiation being shielded. For example, bismuth and lead are commonly used for shielding against gamma and X-rays [3], while concrete or water can be used for shielding against neutron radiation [4,5].

Glass composites doped with heavy elements or mixed with cement are also used for gamma and neutron shielding [6–9].

Radiation shielding is critical in a variety of settings, including medical facilities, nuclear power plants, and research laboratories. Without adequate shielding, workers and the general public could be exposed to dangerous levels of radiation, leading to serious health consequences. Therefore, proper radiation-shielding design and implementation are crucial to ensure the safety of workers, the public, and the environment.

Polymers and rubber-based composites can also be used for radiation shielding. These composites are typically made by combining rubber with other materials, such as lead or tungsten, to create a material that can effectively block both beta and gamma radiation [10–12]. Polymers are an ideal option for radiation shielding because of their lightweight, strong, and flexible properties, as well as their resistance to physical, mechanical, and radiation damage. They are a superior alternative to concrete and lead for radiation shielding. Furthermore, by adding high atomic number materials, polymers can be easily transformed into composites that are more effective as radiation shields [13–15].

Silicone rubber doped with high-atomic-number materials such as lead, cadmium, and tungsten can be used in various applications such as medical imaging, nuclear power plants, and aerospace [16–18]. The effectiveness of the shielding material depends on the composition and thickness of the material, as well as the energy of the radiation being shielded. It is important to note that while silicone rubber doped with lead or tungsten can be effective for radiation shielding, it may not be the best choice for all applications. Factors such as weight, flexibility, and durability may also need to be considered. Ethylene propylene diene monomer (EPDM) rubber composites have the potential to serve as flexible, durable, and lead-free gamma-ray-shielding materials when metal oxides such as iron (II, III) oxide ( $\text{Fe}_3\text{O}_4$ ), tungsten (III) oxide ( $\text{W}_2\text{O}_3$ ), or bismuth (III) oxide ( $\text{Bi}_2\text{O}_3$ ) are added to them [19]. Due to its high boron content, EPDM/Hexagonal boron nitride (hBN) samples are able to attenuate thermal neutron radiation up to 61.5% [20].

Recently, silica fillers have been introduced as a reinforcing filler for rubbers from economic factors as well as their ability to give major benefits, such as low thermal expansion, chemical resistance, hard surface, and high dielectric strength [21]. Exposure to gamma radiation can lead to the creation of point defects in  $\text{SiO}_2$ , such as oxygen vacancies or oxygen interstitials. These defects can induce structural changes in the material, altering its density, crystallinity, and morphology. Such changes can affect the shielding parameters of the NR/NBR blend. However, it is crucial to consider that the precise nature of this impact is contingent upon several factors, such as the concentrations of  $\text{SiO}_2$  and the shielding filler material such as  $\text{Bi}_2\text{O}_3$ , the radiation dosage, and the specific characteristics of the resulting point defects [22].

Nitrile rubber (NBR) is a synthetic elastomer that is commonly used in automotive applications due to its good resistance to oil and low gas permeability, but its limited ageing resistance may require careful consideration in certain situations [22]. Its good radiation resistance also makes it useful in certain specialized applications [23].

The objective of the present study is to create a novel composite material for shielding purposes using a blend of NBR and NR as the matrix. Bismuth oxide will be added to this blend as a filler, and its effect on the mechanical and shielding properties of the composite will be examined. The optimal concentration of bismuth in the blend will also be determined. The new composite material is expected to possess unique physical, mechanical, and attenuation characteristics, as well as being lightweight, affordable, and having reasonable radiation resistance. As a result, it has the potential to be utilized in the production of radiation protection equipment for use by medical, industrial, and military personnel.

## 2. Materials and Methods

### 2.1. Materials

All the rubber components were acquired from Aldrich Co. and were of commercial quality. Table 1 shows how all the used ingredients of the prepared NR/NBR/Bi<sub>2</sub>O<sub>3</sub> composites. The chosen rubber matrix is acrylonitrile butadiene rubber (NBR) and natural rubber (NR). Acrylonitrile butadiene rubber (NBR) containing 32% acrylonitrile content with specific gravity 1.17 + 0.005 was supplied from Bayer AG, Germany. Natural rubber ribbed smoked sheet (Grade RSS 1) is obtained from Transport and Engineering, Alexandria company, Egypt. Its mass density is 0.913 ± 0.005 g/cm<sup>3</sup> at 23 °C, T<sub>g</sub> = −75 °C, and Mooney viscosity in the range 60–90.

**Table 1.** Ingredients of NR/NBR/Bi<sub>2</sub>O<sub>3</sub> composites.

Ingredients	Amounts (phr) *	Function
Natural rubber (NR)	75	Polymer
Acrylonitrile butadiene rubber (NBR)	25	Polymer
Stearic acid	1	Activators
Zinc oxide (ZnO)	3	Activators
Tetramethyl thiuram disulphide (TMTD)	0.5	Accelerators
N-cyclohexyl-2-benzothiazole sulphenamide (CBS)	1	Accelerators
Polymerized 2,2,4-trimethyl-1,2-dihydroquinoline (TMQ)	1	Antioxidant
Sulfur (S)	2	Vulcanizing agent
Dioctyl phthalate (DOP)	3	Plasticizer
Silica (SiO <sub>2</sub> )	20	Filler
Bismuth oxide (Bi <sub>2</sub> O <sub>3</sub> )	Variable	Gamma attenuator filler

\* Part per hundred parts of rubber.

### 2.2. Preparation of Composites

The rubber blends were created using a two-roll mill that had a diameter of 470 mm and a working distance of 300 mm. The slow roller was set to rotate at 24 revolutions per minute, with a gear ratio of 1:1.4. The mixing process followed ASTM D3182 guidelines, with close attention paid to controlling temperature, nip gap, and the order of adding ingredients.

The vulcanization process was conducted using an electrically heated hydraulic press, which was equipped with an automatic control system. The temperature was maintained at 152 ± 1 °C, while the pressure was set at approximately 4 MPa. Standard methods were used to test the compounded rubber and vulcanizates, including ASTM D2084-11(2012) for determining rheometric characteristics using a Monsanto Rheometer model and an oscillating disc rheometer R-100 (MDR one moving Die Rheometer, TA instruments, New Castle, DE, USA).

### 2.3. Material Characterizations

The Zwick tensile testing machine (model Z010, Ulm, Germany) was utilized to determine the tensile strength and elongation at break. Compressed sheets were first cut into dumbbell-shaped specimens with appropriate punching dies, which had a width of 4 mm, a neck length of 15 mm, and a thickness of 1–1.5 mm, in accordance with ASTM D412 standards [24]. Mechanical property testing was carried out using a crosshead speed of 500 mm/min and a load cell of 10–20, as per the ASTM guidelines. Hardness measurements were obtained using a Shore A durometer (Bareiss, Oberdischingen, Germany), following ASTM D2240. The test specimens were at least 6 mm thick.

Mass density was measured at 25 °C using a standard Archimedes procedure, which was based on a given equation.

$$\rho = \frac{W_a}{W_a - W_b} \rho_b \quad (1)$$

where  $W_a$  is the sample's weight in air,  $W_b$  is the sample's weight in Toluene, and  $\rho_b$  is Toluene density of ( $\rho_b = 0.87 \text{ g/cm}^3$ ).

Furthermore, the evaluation of porosity was conducted using the boiling water technique outlined in ASTM C 20-00 [25]. Porosity refers to the ratio between the volume of voids and the total volume of a given specimen. Employing Archimedes' saturation technique (C20-00, 2015), the water displacement method was used, wherein the mass of porous specimens was measured both when dry and when submerged in water. The apparent porosity (P) can be calculated using the following equation:

$$P, \% = \left[ \frac{W - D}{V} \right] \times 100 \quad (2)$$

where  $W$  represents the saturated mass of the specimen in grams,  $D$  is the dry mass of the specimen in grams, and  $V$  denotes the exterior volume of the specimen in cubic centimeters. To attain a constant dry mass, the specimens were placed in an oven at 105–110 °C for 48 h. Subsequently, the dry specimens were immersed in boiling water for 2 h to obtain the saturated mass.

A Bruker Alpha II spectrometer with KBr pellet technique was used to measure attenuated total reflectance Fourier transform infrared (ATR-FTIR) values at spectral range 400–4000  $\text{cm}^{-1}$ .

The gamma-ray-shielding properties of the created rubber matrix were assessed by measuring the parameters at 0.662 MeV gamma photons, which were emitted from a Cs-137-point source and were placed under appropriate geometrical conditions. A NaI (Tl) scintillation detector (Teledyne Isotopes "2 × 2" NaI (Tl) Scintillation Detector, Alabama, USA) was utilized to conduct the measurements, and it possessed an energy resolution of 8% at 662 keV.

### 3. Theoretical Background

The modified Lambert–Beer Law was employed to compute the linear attenuation coefficients in the following manner [26]:

$$I = I_0 \times B \times e^{-\mu x} \quad (3)$$

where the initial photon intensity ( $I_0$ ) and the transmitted photon intensity ( $I$ ) are related to the linear attenuation coefficient ( $\mu$ ) in units of  $\text{cm}^{-1}$ , while the buildup factor ( $B$ ) is dependent on the thickness ( $x$ ) of the material used and the energy ( $E$ ) of the incident photon. To calculate the mass attenuation coefficient ( $\mu_m$ ), one can use the linear attenuation coefficient and the mass density ( $\rho$ ) values with the following equation [27]:

$$\mu_m = \frac{\mu}{\rho} \quad (4)$$

In the case of a compound or mixture, the following formula can be used to determine  $\mu_m$  [28]:

$$\mu_m = \sum_i w_i (\mu_m)_i \quad (5)$$

where  $(\mu_m)_i$  is the mass attenuation coefficient of the examined mixture's  $i$ th element and  $w_i$  stands for its weight percentage. The half-value layer (HVL) and the mean free path (MFP) of the prepared composites can be calculated by using the following formulas, respectively [29–31]:

$$\text{HVL} = \frac{0.693}{\mu} \quad (6)$$

$$\text{MFP} = \frac{1}{\mu} \quad (7)$$

In order to determine the mass attenuation coefficients of the prepared samples across a wide range of energies from 0.015 to 15 MeV, the National Institute of Standard and Tech-

nology (NIST) developed a photon cross-sections database named XCOM, which includes the attenuation coefficients of all elements in the periodic table at different energies [32].

The ratio of an object's electronic cross-section ( $\sigma_a$ ) to its effective atomic cross-section ( $\sigma_e$ ) is used to define the effective atomic number of a material ( $Z_{\text{eff}}$ ). The obtained data for the mass attenuation coefficient ( $\mu_m$ ) of the produced prepared samples can be utilized with the following formula to estimate the values of  $Z_{\text{eff}}$  [33]:

$$Z_{\text{eff}} = \frac{\sigma_a}{\sigma_e} = \frac{\sum_i f_i A_i (\mu_m)_i}{\sum_i f_i \frac{A_i}{Z_i} (\mu_m)_i} \quad (8)$$

where  $A_i$  is the atomic weight,  $Z_i$  is the atomic number,  $(\mu_m)_i$  is the mass attenuation coefficient for the  $i$ th element, and  $f_i$  represents  $i$ th element fractional abundance concerning the number of atoms.

In order to determine the buildup factor, we need to obtain the Compton partial attenuation coefficient ( $(\mu_m)_{\text{comp}}$ ) and the total attenuation coefficient ( $(\mu_m)_{\text{total}}$ ) values for the constituent elements and compounds present in the prepared samples being analyzed within the energy range of 0.015–15.0 MeV. Using these values, we can then calculate the equivalent atomic number ( $Z_{\text{eq}}$ ) for the produced prepared samples by comparing the ratio  $(\mu_m)_{\text{comp}}/(\mu_m)_{\text{total}}$  at a specific energy with comparable ratios of elements at the same energy. The interpolation of the equivalent atomic number was determined through a logarithmic interpolation algorithm [34], where the ratio  $(\mu_m)_{\text{comp}}/(\mu_m)_{\text{total}}$  falls between two consecutive ratios of elements.

$$Z_{\text{eq}} = \frac{Z_1(\log R_2 - \log R) + Z_2(\log R - \log R_1)}{\log R_2 - \log R_1} \quad (9)$$

The values of  $Z_1$  and  $Z_2$  are the atomic numbers of the pure elements that correspond to the ratios  $R_1$  and  $R_2$ , respectively.  $R$  is the ratio for the prepared samples being studied at certain energy [35]. The exposure buildup factor EBF for the prepared samples was calculated using the general progressive (G-P) interpolation in the energy range of 0.015–15 MeV up to 40 mfp, with the help of the equations provided in Harima et al. (1993) [36–38]:

$$B(E, X) = 1 + \frac{b-1}{K-1}(K^X - 1) \quad \text{for } K \neq 1 \quad (10)$$

$$B(E, X) = 1 + (b-1)X \quad \text{for } K = 1 \quad (11)$$

$$K(E, X) = cX^a + d \frac{\tanh\left(\frac{X}{X_K} - 2\right) - \tanh(-2)}{1 - \tanh(-2)} \quad (12)$$

These formulas involve several variables such as photon energy ( $E$ ), separation ( $X$ ) between detector and source, exposure buildup factor (EBF) value at 1 mean free path (MFP) denoted by  $B$ , dosage multiplicative factor ( $K$ ), and several fitting parameters ( $b$ ,  $c$ ,  $a$ ,  $X_K$ , and  $d$ ) that are dependent on the attenuating medium and source energy. The fitting parameters for the prepared samples, namely  $b$ ,  $c$ ,  $a$ ,  $X_K$ , and  $d$ , can be estimated for the energy range of gamma rays from 0.015 MeV to 15 MeV, up to a distance of 40 MFP, using logarithmic interpolation with the help of the following equation-like method [39,40].

$$P = \frac{P_1(\log Z_2 - \log Z_{\text{eq}}) + P_2(\log Z_{\text{eq}} - \log Z_1)}{\log Z_2 - \log Z_1} \quad (13)$$

The values of the G-P fitting parameters at specific energy for atomic numbers  $Z_1$  and  $Z_2$  are denoted by  $P_1$  and  $P_2$ , respectively. The criteria for the G-P fit for the elements, as established by the American Nuclear Society study, were applied [41].

## 4. Results and Discussion

### 4.1. NR/NBR Blend

Five blends of NR/NBR are prepared according to the compounding formulations for NR and NBR blends with peroxide for optimum blend ratio as shown in Table 2. Rheometric characteristics of these blends are investigated, and the blend of the best mechanical properties will be used to be loaded with bismuth oxide to enhance the blend's radiation-shielding characteristics. The rheometric characteristics of the prepared NR/NBR blends cured with 3phr peroxide are shown in Table 3.

**Table 2.** The formulations of NR/NBR blends.

	N1	N2	N3	N4	N5
NR (phr)	-	25	50	75	100
NBR (phr)	100	75	50	25	-
Peroxide(phr)	3	3	3	3	3

**Table 3.** Rheometric characteristics of NR/NBR blends cured with 3phr peroxide.

Rheometric Characteristics	N1	N2	N3	N4	N5
$M_L$ (dN.m)	0.62	0.61	0.45	0.53	0.78
$M_H$ (dN.m)	10.42	9.32	8.5	7.95	7.35
$T_{c90}$ (min)	16.15	16.5	16.53	16.6	16.31
$T_{s2}$ (min)	2.47	3.22	3.4	3.67	3.56
CIR ( $\text{min}^{-1}$ )	7.31	7.53	7.62	7.73	7.84

minimum torque ( $M_L$ ), maximum torque ( $M_H$ ), optimum cure time ( $T_{c90}$ ), scorch time ( $T_{s2}$ ), cure rate index (CRI).

The obtained data regarding the mechanical properties of the five NR/NBR prepared blends are shown in Figure 1, where N4 (75/25 phr) showed the highest tensile strength and elongation. These results can be attributed to the nature of the blend which has a highly interconnected two-phase morphology.

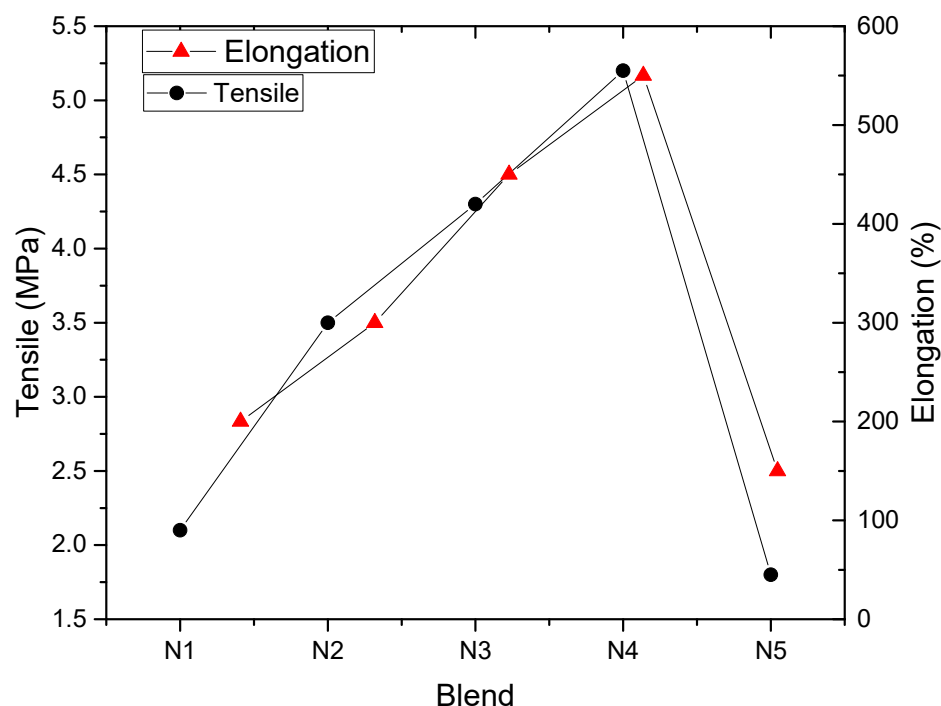


**Figure 1.** Mechanical properties of NR/NBR blend.

#### 4.2. NR/NBR/Bi<sub>2</sub>O<sub>3</sub> Matrix (Composites)

Accordingly, the blend ratio 75/25 NR/NBR was chosen to be incorporated with different concentrations of Bi<sub>2</sub>O<sub>3</sub> (0–45 phr) to test the shielding blend properties in the rubber composite formulations.

The mass density of NR/NBR/Bi<sub>2</sub>O<sub>3</sub> blend increases proportionally with increasing bismuth ratio as shown in Table 4. The vulcanization of NR/NBR/Bi<sub>2</sub>O<sub>3</sub> was carried out using peroxide as a curing agent. The rheometric characteristics blends were determined at 152 °C and listed in Table 5.

**Table 4.** Density of NR/NBR/Bi<sub>2</sub>O<sub>3</sub> matrix.

	Sample No.									
	N0	N1	N2	N3	N4	N5	N6	N7	N8	N9
Bi <sub>2</sub> O <sub>3</sub> (phr)	0	5	10	15	20	25	30	35	40	45
Density (g/cm <sup>3</sup> )	2.326	2.864	2.911	3.012	3.142	3.251	3.624	3.653	3.709	3.741

**Table 5.** Rheometric characteristics of NR/NBR/Bi<sub>2</sub>O<sub>3</sub> composites at (152 ± 1) °C.

Rheometric Characteristics	Samples No.									
	N0	N1	N2	N3	N4	N5	N6	N7	N8	N9
M <sub>L</sub> (dN.m)	1.14	0.93	0.85	0.82	0.77	0.79	0.83	0.89	0.89	0.89
M <sub>H</sub> (dN.m)	10.22	12.33	14.48	15.76	18.01	17.58	17.2	16.8	16.3	16.2
T <sub>c90</sub> (min)	3.56	3.58	3.87	4.46	5.17	6.29	6.44	6.86	6.97	7.01
T <sub>s2</sub> (min)	1.94	1.83	1.74	1.70	1.65	1.54	1.51	1.45	1.41	1.33
CIR (min <sup>-1</sup> )	61.73	57.14	46.94	36.23	28.41	21.05	20.28	18.48	17.98	17.60

minimum torque (M<sub>L</sub>), maximum torque (M<sub>H</sub>), optimum cure time (T<sub>c90</sub>), scorch time (T<sub>s2</sub>), cure rate index (CRI).

As illustrated in Table 5, the maximum torque (M<sub>H</sub>) initially increased with bismuth concentration due to the crosslinking that occurred while the subsequent decrease refers to the degradation that happened in the blend composites. The observed decrease in scorch time with the increase in bismuth concentration indicates how quickly the material begins to vulcanize with adding bismuth. Following the addition of bismuth, the vulcanization of the NR/NBR mix is accelerated as a result of the interaction between bismuth and the vulcanization system. By encouraging the cross-linking of rubber molecules and accelerating the vulcanization process, bismuth increases the effectiveness of curing in general. As a result, the mix vulcanizes more quickly and completely, giving the vulcanized product more strength, stability, and other desirable qualities [42].

#### 4.3. Total Reflectance Fourier Transform Infrared (ATR-FTIR)

The absorbance spectra of NR/NBR/ Bi<sub>2</sub>O<sub>3</sub> with different concentrations of bismuth oxide are shown in Figure 2. The peak positions and their assignment vibrational modes are shown in Table 6.

**Table 6.** Assignment of Infrared bands in the spectra of the prepared composite samples.

Peak Position (cm <sup>-1</sup> )	Assignment	Reference Range
3320	OH stretching vibrations	3330–3353 [43–45]
2958	C-H <sub>3</sub> symmetric stretching	2950–2960 [46]
2917	C-H <sub>3</sub> asymmetric stretching vibration	2910–2920 [46]
2850	Asymmetric C-H <sub>2</sub> stretching vibration modes	2850–2860 [46]
2726	Stretching vibration of C-H groups	3000–2500 [47]
1731	C=O stretching vibration carbonyl group	1725–1740 [46–48]

Table 6. Cont.

Peak Position (cm <sup>-1</sup> )	Assignment	Reference Range
1625	Stretching vibration of C=C groups	1600–1580 [46]
1539	N=O stretching vibration	1585–1539 [46]
1450	C-H <sub>3</sub> bending vibration	1470–1410 [46]
1396	Stretching vibration of C-N groups	1400–1300 [32]
1375	Stretching vibration of C-H groups	1460–1340 [32]
1311	Stretching vibration of C-N groups	1400–1200 [46]
1086	C-O chain stretching	1050–1300 [46,49,50]
900	Si-H stretching	800–950 [46]
832	Bending vibration of C-H groups	900–625 [47]
742	Bending vibration of C-H groups	900–625 [47]
643	Bending vibration of C-H groups	900–625 [47]
566	Out-of-plane bending of the C-H bond in the CH <sub>2</sub> group	600–500 [45]
462	Metal–ligand stretching vibration such as Bi-O, Zn-O and Zn-CH <sub>3</sub> stretching vibrations	400–600 [51,52]

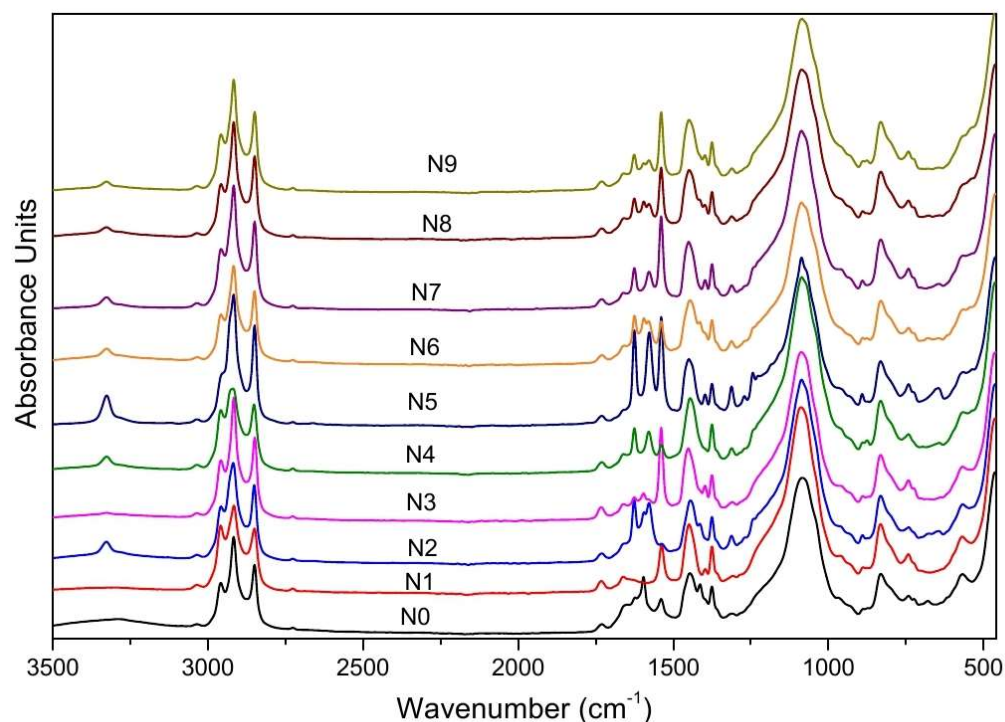


**Figure 2.** Attenuated total reflection Fourier transform infrared spectroscopy analysis of NR/NBR/Bi<sub>2</sub>O<sub>3</sub> composites.

#### 4.4. Mechanical Properties of NR/NBR/Bi<sub>2</sub>O<sub>3</sub> Composites

The impact of the presence of bismuth filler on the mechanical characteristics of the NR/NBR/Bi<sub>2</sub>O<sub>3</sub> composites was evaluated, and the results are depicted in Figures 3–5. The outcomes revealed that the incorporation of bismuth led to an enhancement in tensile strength, elongation, and hardness. The tensile strength and elongation of the base material increased as the filler loading increased up to 20 phr, after which they slightly decreased as the bismuth concentration rose.

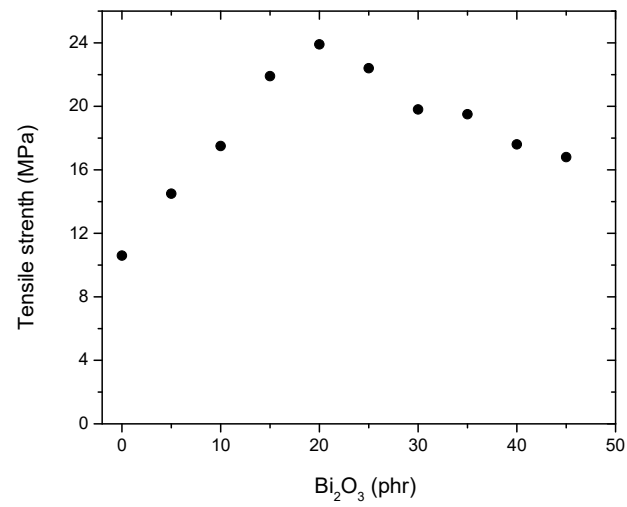


**Figure 3.** Effect of Bismuth content on the tensile strength of NR/NBR/Bi<sub>2</sub>O<sub>3</sub> composites.

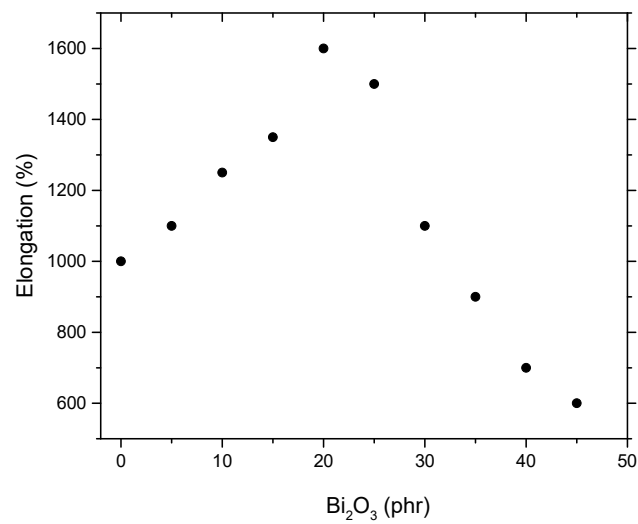


**Figure 4.** Effect of filler content on the elongation of the NR/NBR/Bi<sub>2</sub>O<sub>3</sub> composites.

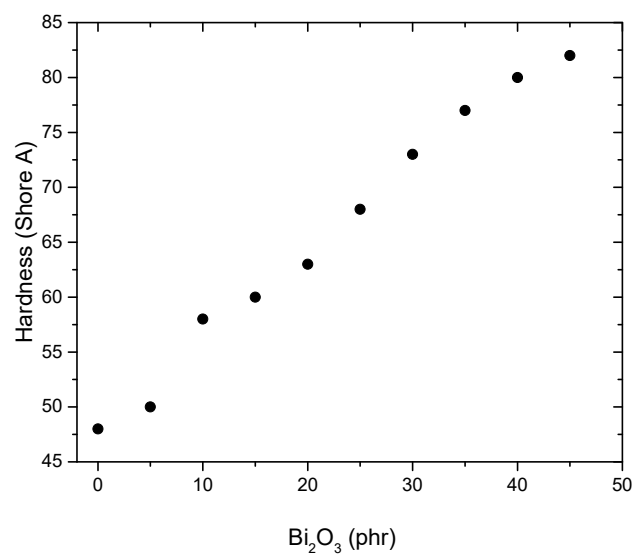


**Figure 5.** Effect of filler content on the hardness (Shore A) of NR/NBR/Bi<sub>2</sub>O<sub>3</sub> composites.

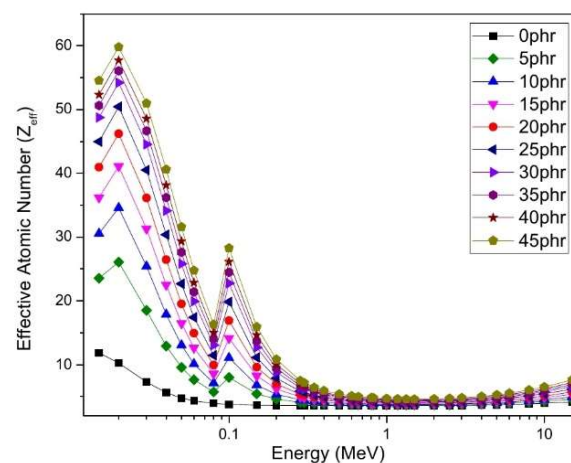
Adding  $\text{Bi}_2\text{O}_3$  to the rubber blend (NR/NBR) can improve mechanical properties such as tensile strength, hardness, and maximum elongation. This is due to the following reasons: Bismuth is a high-density material ( $9.78 \text{ g/cm}^3$ ), which increases the overall density of the rubber blend. As a result, the intermolecular forces between the polymer chains and the filler particles become stronger, leading to an increase in the tensile strength of the blend [53,54]. Bismuth also has a relatively high modulus of elasticity compared to other fillers, which can increase the stiffness and hardness of the rubber blend. This can be particularly useful in radiation-shielding applications where the material needs to be rigid and maintain its shape under exposure to high radiation doses. Bismuth has a low coefficient of thermal expansion, which means that it does not expand or contract much with changes in temperature. This property can prevent the filler particles from separating from the polymer matrix, which can improve the maximum elongation of the blend.

While adding  $\text{Bi}_2\text{O}_3$  to the natural rubber/nitrile butadiene rubber (NR/NBR) blend can improve the mechanical properties, increasing the concentration of  $\text{Bi}_2\text{O}_3$  beyond a 20 phr can lead to a decrease in these properties. This can be explained as follows: At high concentrations, Bi particles can agglomerate, causing the formation of clusters that reduce the intermolecular forces between the polymer chains and the filler particles. This reduces the strength of the polymer–filler interface, leading to a decrease in the tensile strength of the blend [11]. Moreover,  $\text{Bi}_2\text{O}_3$  is a relatively brittle material, and increasing its concentration can make the blend more prone to cracking and fracture. This can reduce the maximum elongation and toughness of the blend, making it less suitable for applications where flexibility and impact resistance are required.

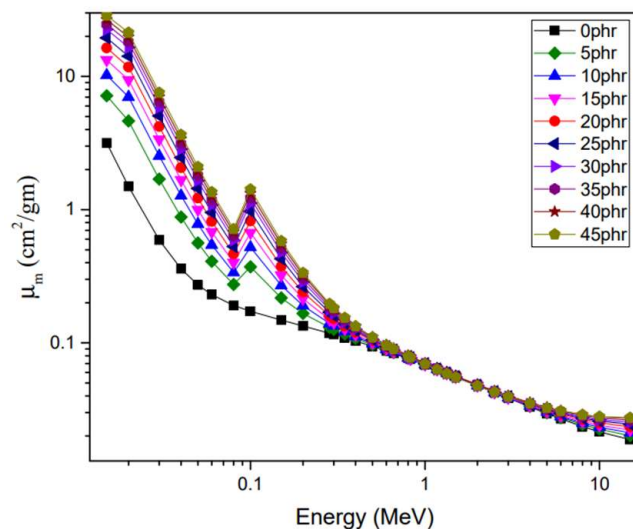
Therefore, it is essential to carefully control the concentration of  $\text{Bi}_2\text{O}_3$  in the NR/NBR blend and optimize the processing conditions to achieve the desired mechanical properties.

#### 4.5. Gamma-Ray-Shielding Properties of NR/NBR/ $\text{Bi}_2\text{O}_3$ Composites

Figures 6 and 7 show the results of  $Z_{\text{eff}}$  and  $\mu_{\text{m}}$  of the prepared rubber matrix at the energy range 0.015–15 MeV, respectively. The variation profile of  $Z_{\text{eff}}$  with energy for different  $\text{Bi}_2\text{O}_3$  concentrations was almost the same but shifted to higher values. As previously reported [55], photoelectric interaction is proportional to  $Z^{4-5}$  for attenuation, while Compton interaction and pair production are proportional to  $Z$  and  $Z^2$ , respectively. This could cause a realized increase in the effective atomic numbers with the  $\text{Bi}_2\text{O}_3$  concentration (phr) increment. Moreover, during the vulcanization process, the rubber mixture is heated, and the bismuth compounds decompose, releasing bismuth ions ( $\text{Bi}^{3+}$ ). These ions can then react with the rubber molecules and form chemical bonds, which help to strengthen the rubber network. The bismuth ions can also react with other elements in the mixture, such as sulfur and zinc oxide, to form crosslinks that further reinforce the rubber network and cause a distinct increase in both  $Z_{\text{eff}}$  and  $\mu_{\text{m}}$ .



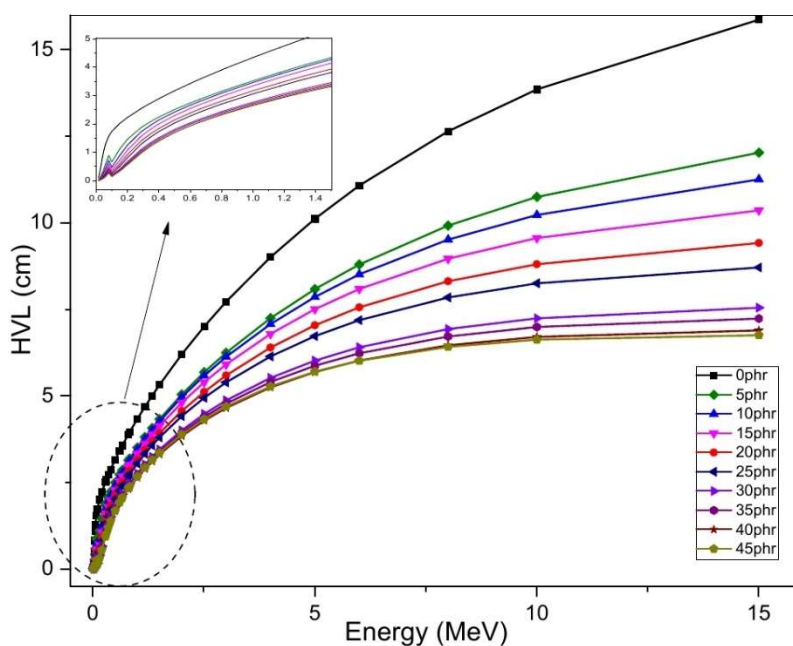
**Figure 6.** Effective atomic numbers for NR/NBR/ $\text{Bi}_2\text{O}_3$  rubber matrix.



**Figure 7.** Mass attenuation coefficients for NR/NBR blend with different concentrations of Bismuth Oxide.

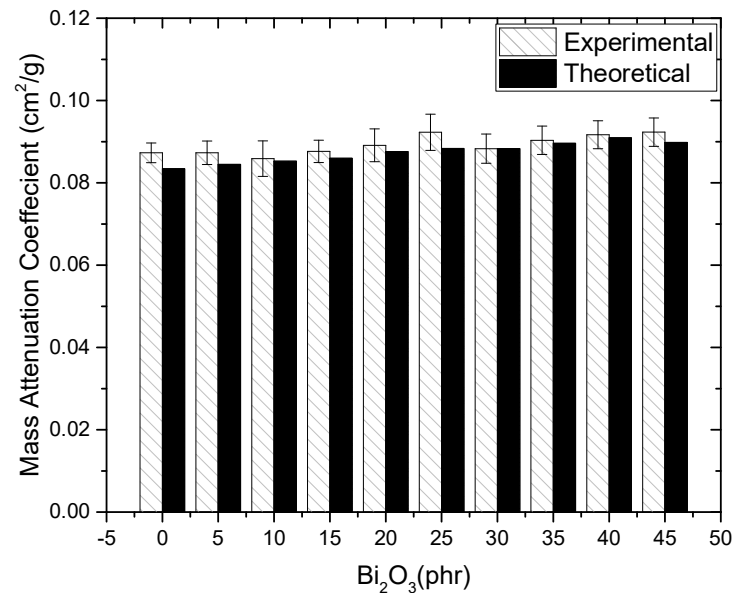
When the incident photon energy is in the low-energy range of about 0.1 MeV, where the photoelectric interaction dominates,  $Z_{eff}$  increases in all samples. The highest value of  $Z_{eff}$  is observed at about 0.091 MeV due to the K-edge of  $Bi_2O_3$  absorption [56]. However, as photoelectric absorption decreases and Compton scattering becomes more dominant in the energy range of 0.1–1 MeV, there is a sharp decrease in  $Z_{eff}$ . Pair production interaction is the most dominant from 1–15 MeV, and the interaction probability is directly proportional to the energy. These findings are consistent with the fundamental concepts of gamma photon interaction probability, which is directly proportional to the effective atomic number of the matrix and inversely proportional to photon energy. The effect of increasing  $Bi_2O_3$  (phr) and energy on  $Z_{eff}$  variation is similar to that on  $\mu_m$ . Figures 6 and 7 depict this relationship.

Figure 8 shows that the half-value layer (HVL) increases with energy for NR/NBR/ $Bi_2O_3$  rubber composites. The change in  $Z_{eff}$  with  $Bi_2O_3$  concentration and photon energy is consistent with the results obtained for  $\mu_m$  and the corresponding HVL.



**Figure 8.** Half-value layer (HVL) results for NR/NBR blend with different phr  $Bi_2O_3$ .

Figure 9 shows a comparison between the calculated values of the mass attenuation coefficient ( $\mu_m$ ) and the values measured at 0.662 MeV. The measured values show good agreement with the theoretical values, with a difference of up to 4%.



**Figure 9.** Experimental and theoretical mass attenuation coefficients of the prepared samples at 0.662 MeV.

The energy buildup factor (EBF) results were obtained by considering the concentration of Bi<sub>2</sub>O<sub>3</sub>, photon energy, and penetration depth as factors that influence EBF. Figure 10a–j indicate that the EBF has the lowest values in the low- and high-energy regions where complete absorption of a photon occurs during photoelectric interactions at low energy and pair production interactions at high energy. Conversely, the intermediate energy region is characterized by Compton scattering interactions, resulting in higher EBF values [57].

The presence of a peak at 0.08 MeV followed by a valley at 0.1 MeV for Bi<sub>2</sub>O<sub>3</sub> doped samples can be explained by the absorption K-edge of Bi<sub>2</sub>O<sub>3</sub>, which is around 0.1 MeV (0.091 MeV). An increase in Bi<sub>2</sub>O<sub>3</sub> concentration raises the mass attenuation coefficient, thereby reducing the penetration depth. When penetration depth is large, multiple scattering events occur, leading to an increase in the thickness of the interacting substance, and resulting in more scattering events and higher EBF values. Therefore, EBF is directly proportional to penetration depth and inversely proportional to Bi<sub>2</sub>O<sub>3</sub> concentration.

#### 4.6. Neutron Attenuation

The fast neutron removal cross-section, also called the “macroscopic cross-section”, measures the likelihood that a fast or fission energy neutron will be removed from a group of uncollided neutrons due to its first collision [58]. In Figure 11, the calculated mass removal cross-sections ( $\Sigma_R$ ) of the prepared samples for fast neutrons are displayed. As the concentration of Bi<sub>2</sub>O<sub>3</sub> increases, the mass removal cross-section of the samples decreases continuously, which can be attributed to the reduction in the weight fraction of hydrogen content. The mass removal cross-section values obtained ranged from 0.092–0.072 cm<sup>2</sup>/g, corresponding to the variation of Bi<sub>2</sub>O<sub>3</sub> concentration from 0–45 phr. In comparison to the commonly utilized B<sub>4</sub>C with a neutron mass removal cross-section of 0.0559 cm<sup>2</sup>/g, the prepared blend exhibits potential for diverse neutron-shielding applications and is, therefore, a recommended choice.

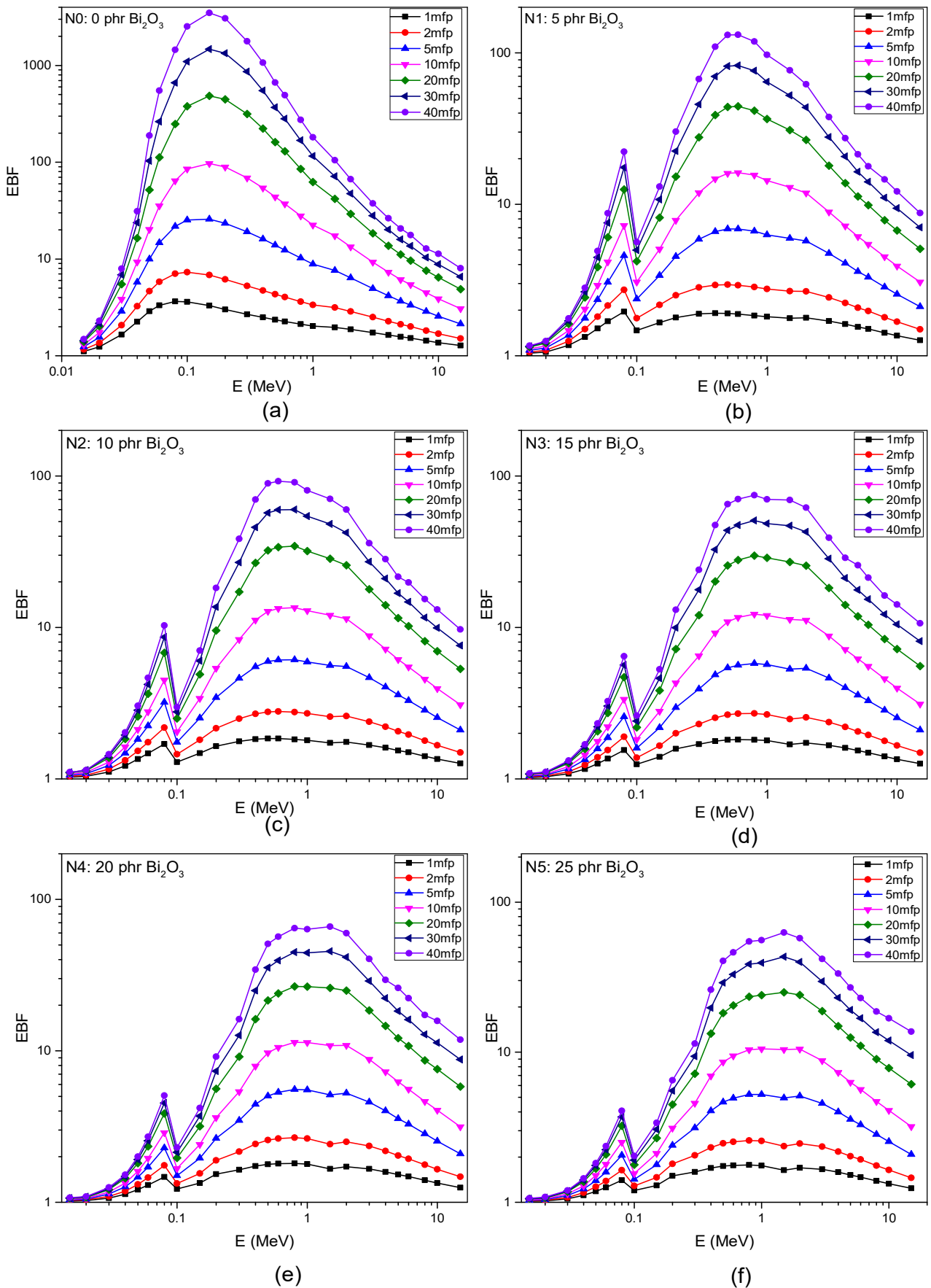
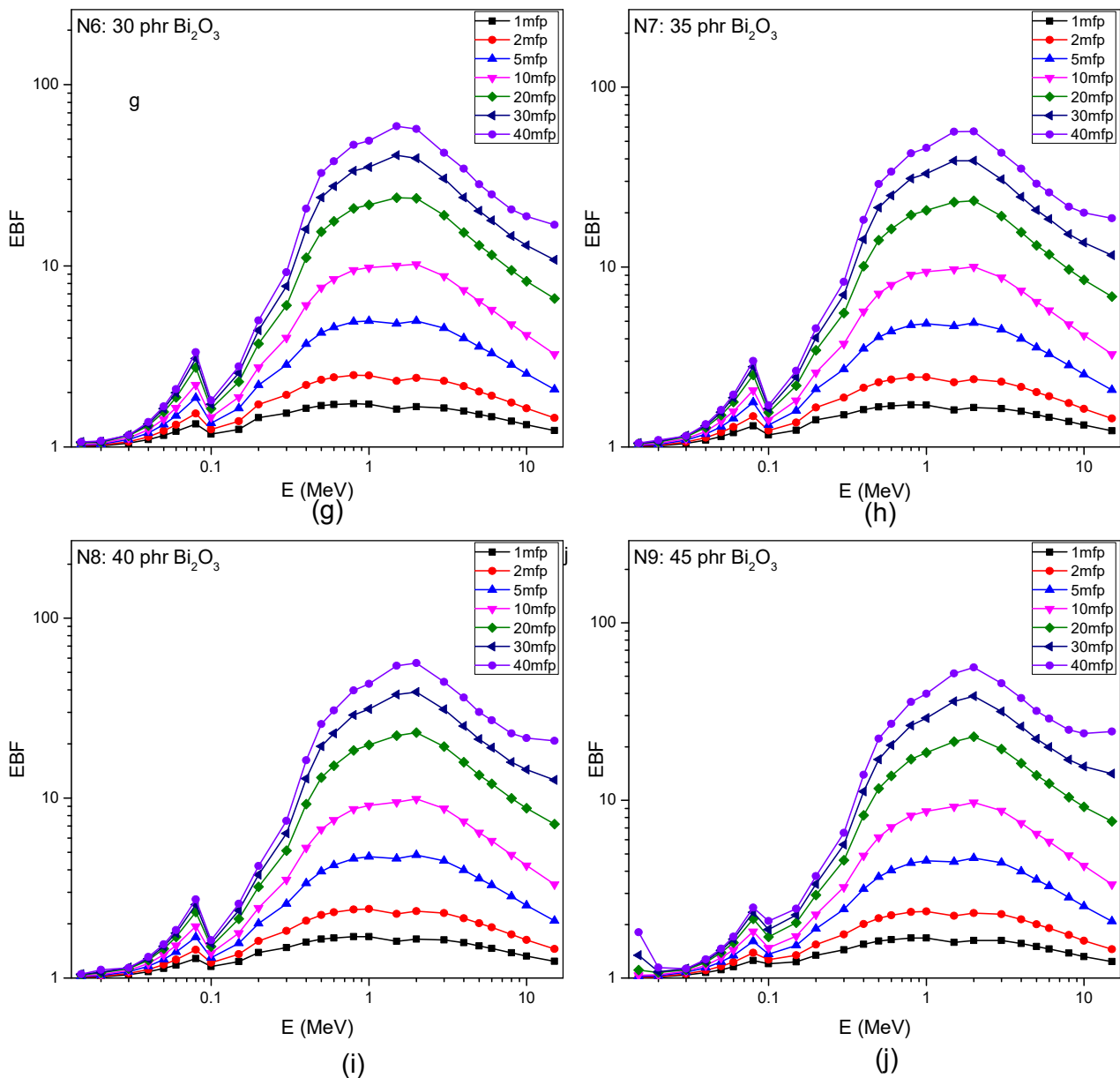


Figure 10. Cont.



**Figure 10.** EBF of NR/NBR/ $\text{Bi}_2\text{O}_3$  blend at energy range from 0.015–15 MeV up to 40 mfp for different concentrations of  $\text{Bi}_2\text{O}_3$ : (a) zero phr, (b) 5 phr, (c) 10 phr, (d) 15 phr, (e) 20 phr, (f) 25 phr, (g) 30 phr, (h) 35 phr, (i) 40 phr, (j) 45 phr.

#### 4.7. The Effect of Gamma Irradiation and Porosity

Figure 12 shows the effect of gamma irradiation doses on NR/NBR/20 phr  $\text{Bi}_2\text{O}_3$  composite's porosity. The observed increase in the rubber composite porosity with an increase in gamma irradiation dose can be explained by the effects of radiation on the polymer structure. When rubber is exposed to gamma radiation, high-energy photons interact with the polymer chains, causing various chemical and physical changes [59]. One of the primary mechanisms leading to increased porosity is chain scission. Gamma radiation can break the polymer chains, resulting in the formation of free radicals and smaller molecular fragments. As the radiation dose increases, the number of chain scissions also increases. The presence of these broken chains weakens the overall structure of the rubber and creates spaces or voids within the material, leading to increased porosity.

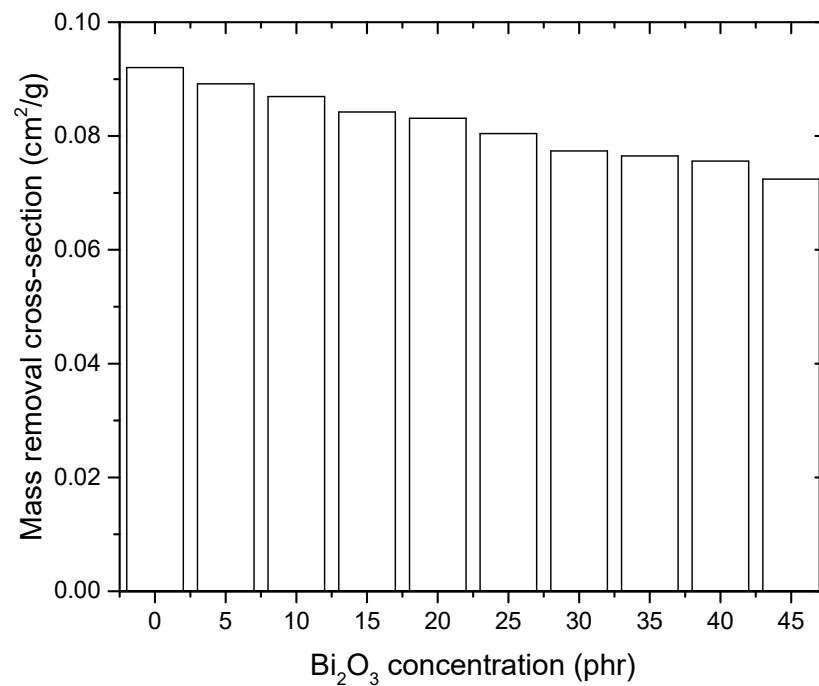


**Figure 11.** Fast neutron mass removal cross-sections (cm<sup>2</sup>/g) for NR/NBR blend at different concentrations of Bi<sub>2</sub>O<sub>3</sub>.

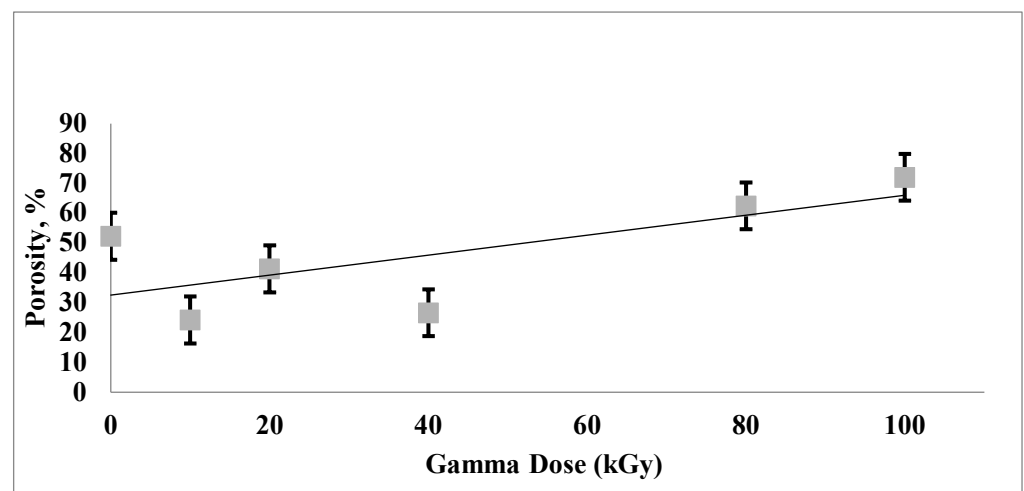


**Figure 12.** The effect of gamma irradiation doses on NR/NBR/20 phr Bi<sub>2</sub>O<sub>3</sub> composite's porosity.

Moreover, gamma irradiation has an additional impact on rubber known as crosslinking. While chain scission causes the breakdown of polymer chains, crosslinking creates new bonds between these chains [60]. However, when exposed to higher radiation doses, the crosslinking density may initially increase until reaching a maximum, after which it begins to decrease due to recombination reactions and the formation of new free radicals. This decrease in crosslinking density can result in an elevation of rubber porosity. Additionally, the degradation induced by radiation can generate volatile by-products. These by-products have the potential to escape from the rubber matrix, leaving behind voids or pores that contribute to the overall increase in porosity. The obtained results of porosity increase with the radiation exposure indicating that the shielding capability of the prepared blend is decreasing with the gamma exposure doses. This means the aging effect of this material could be considered.

## 5. Conclusions

This study aimed to develop the optimum NR/NBR blend by adding different concentrations of  $\text{Bi}_2\text{O}_3$  for gamma- and neutron-shielding applications. The obtained results showed that the NR/NBR blend of 75/25 phr had the maximum tensile strength and elongation. This blend is considered the optimum NR/NBR blend to be incorporated with different concentrations of  $\text{Bi}_2\text{O}_3$  (0–45 phr) for the preparation of radiation shielding composites. The mechanical and shielding properties of the NR/NBR/ $\text{Bi}_2\text{O}_3$  composites were investigated. Although the mass attenuation coefficient and other shielding parameters increased with the addition of bismuth, the most recommended composite was that at 20 phr  $\text{Bi}_2\text{O}_3$ , where the maximum tensile strength and elongation were obtained. This study analyzed the exposure build-up factors (EBF) of composite materials that were prepared with varying concentrations of  $\text{Bi}_2\text{O}_3$ . The analysis was conducted for photon energies ranging from 0.015 to 15 MeV and penetration depths up to 40 mfp. Additionally, this study also evaluated the fast neutron mass removal cross-sections of the prepared composites using the partial density approach to determine their potential for attenuating neutrons. Overall, the addition of bismuth to the rubber blend can improve the mechanical properties and make it more suitable for radiation-shielding applications. However, the optimal amount of bismuth and the processing conditions need to be carefully controlled to achieve the desired properties. Moreover, the age of using the prepared blend should take into account the decrease in the shielding capability due to the effect of gamma exposure on its porosity.

**Author Contributions:** Methodology, O.A., E.S. and D.E.E.-N.; Formal analysis, E.S.; Writing—original draft, O.A. and E.S.; Writing—review & editing, E.S. and D.E.E.-N.; Supervision, E.S., D.E.E.-N. and A.B. All authors have read and agreed to the published version of the manuscript.

**Funding:** This research received no external funding.

**Institutional Review Board Statement:** Not applicable.

**Informed Consent Statement:** Not applicable.

**Data Availability Statement:** Not applicable.

**Conflicts of Interest:** The authors declare no conflict of interest.

## References

1. More, C.V.; Alavian, H.; Pawar, P.P. Evaluation of gamma-ray attenuation characteristics of some thermoplastic polymers: Experimental, WinXCom and MCNPX studies. *J. Non Cryst. Solids* **2020**, *546*, 120277. [[CrossRef](#)]
2. Nambiar, S.; Yeow, J.T.W. Polymer-composite materials for radiation protection. *ACS Appl. Mater. Interfaces* **2012**, *4*, 5717–5726. [[CrossRef](#)] [[PubMed](#)]
3. Sayyed, M.I.; El-Mesady, I.A.; Abouhaswa, A.S.; Askin, A.; Rammah, Y.S. Comprehensive study on the structural, optical, physical and gamma photon shielding features of  $\text{B}_2\text{O}_3$ - $\text{Bi}_2\text{O}_3$ - $\text{PbO}$ - $\text{TiO}_2$  glasses using WinXCOM and Geant4 code. *J. Mol. Struct.* **2019**, *1197*, 656–665. [[CrossRef](#)]
4. Ambika, M.R.; Nagaiah, N.; Suman, S.K. Role of bismuth oxide as a reinforcer on gamma shielding ability of unsaturated polyester based polymer composites. *J. Appl. Polym. Sci.* **2017**, *134*, 44657. [[CrossRef](#)]
5. Saleh, H.M.; Bondouk, I.I.; Salama, E.; Esawii, H.A. Consistency and shielding efficiency of cement-bitumen composite for use as gamma-radiation shielding material. *Prog. Nucl. Energy* **2021**, *137*, 103764. [[CrossRef](#)]
6. Esawii, H.A.; Salama, E.; Sayed El-ahll, L.; Moustafa, M.; Saleh, H.M. High impact tungsten-doped borosilicate glass composite for gamma and neutron transparent radiation shielding. *Prog. Nucl. Energy* **2022**, *150*, 104321. [[CrossRef](#)]
7. Ehab, M.; Salama, E.; Ashour, A.; Attallah, M.; Saleh, H.M. Optical Properties and Gamma Radiation Shielding Capability of Transparent Barium Borosilicate Glass Composite. *Sustainability* **2022**, *14*, 13298. [[CrossRef](#)]
8. Eid, M.S.; Bondouk, I.I.; Saleh, H.M.; Omar, K.M.; Sayyed, M.I.; El-Khatib, A.M.; Elsafi, M. Implementation of waste silicate glass into composition of ordinary cement for radiation shielding applications. *Nucl. Eng. Technol.* **2022**, *54*, 1456–1463. [[CrossRef](#)]
9. Eid, M.S.; Bondouk, I.I.; Saleh, H.M.; Omar, K.M.; Diab, H.M. Investigating the Effect of Gamma and Neutron Irradiation on Portland Cement Provided with Waste Silicate Glass. *Sustainability* **2023**, *15*, 763. [[CrossRef](#)]
10. Welborn, D.; Lockwood, P. Lead-rubber shielding effect on radiation dose to the gonads from a bilateral hand X-ray examination. *Radiography* **2022**, *28*, 360–365. [[CrossRef](#)]

11. Intom, S.; Kalkornsuraprane, E.; Johns, J.; Kaewjaeng, S.; Kothan, S.; Hongtong, W.; Chaiphaksa, W.; Kaewkhao, J. Mechanical and radiation shielding properties of flexible material based on natural rubber/Bi<sub>2</sub>O<sub>3</sub> composites. *Radiat. Phys. Chem.* **2020**, *172*, 108772. [[CrossRef](#)]
12. Kalkornsuraprane, E.; Kothan, S.; Intom, S.; Johns, J.; Kaewjaeng, S.; Kedkaew, C.; Chaiphaksa, W.; Sareein, T.; Kaewkhao, J. Wearable and flexible radiation shielding natural rubber composites: Effect of different radiation shielding fillers. *Radiat. Phys. Chem.* **2021**, *179*, 109261. [[CrossRef](#)]
13. Yılmaz, S.N.; Güngör, A.; Özdemir, T. The investigations of mechanical, thermal and rheological properties of polydimethylsiloxane/bismuth (III) oxide composite for X/Gamma ray shielding. *Radiat. Phys. Chem.* **2020**, *170*, 108649. [[CrossRef](#)]
14. Özdemir, T.; Yılmaz, S.N. Mixed radiation shielding via 3-layered polydimethylsiloxane rubber composite containing hexagonal boron nitride, boron (III) oxide, bismuth (III) oxide for each layer. *Radiat. Phys. Chem.* **2018**, *152*, 17–22. [[CrossRef](#)]
15. Saleh, H.M.; Bondouk, I.I.; Salama, E.; Mahmoud, H.H.; Omar, K.; Esawii, H.A. Asphaltene or Polyvinylchloride Waste Blended with Cement to Produce a Sustainable Material Used in Nuclear Safety. *Sustainability* **2022**, *14*, 3525. [[CrossRef](#)]
16. Luan, W.; Wang, Q.; Sun, Q.; Lu, Y. Preparation of CF/Ni-Fe/CNT/silicone layered rubber for aircraft sealing and electromagnetic interference shielding applications. *Chin. J. Aeronaut.* **2021**, *34*, 91–102. [[CrossRef](#)]
17. Wei, H.; Lou, L.; Yang, Z.; He, R.; Fan, J.; Zhang, K.; Yang, W. Multifunctional composites silicone rubber/paraffin@lead tungstate with different core/shell ratio for thermal regulation and gamma shielding. *J. Energy Storage* **2021**, *36*, 102363. [[CrossRef](#)]
18. Wang, J.; Zhou, H.; Gao, Y.; Xie, Y.; Zhang, J.; Hu, Y.; Wang, D.; You, Z.; Wang, S.; Li, H.; et al. The characterization of silicone-tungsten-based composites as flexible gamma-ray shields. *Materials* **2021**, *14*, 5970. [[CrossRef](#)]
19. Poltabtim, W.; Wimolmala, E.; Saenboonruang, K. Properties of lead-free gamma-ray shielding materials from metal oxide/EPDM rubber composites. *Radiat. Phys. Chem.* **2018**, *153*, 1–9. [[CrossRef](#)]
20. Güngör, A.; Akbay, I.K.; Özdemir, T. EPDM Rubber with hexagonal Boron Nitride: A Thermal Neutron Shielding Composite. *Radiat. Phys. Chem.* **2019**, *165*, 108391. [[CrossRef](#)]
21. White, J.L.; Kim, K.J. *Thermoplastic and Rubber Compounds: Technology and Physical Chemistry*; Hanser: Munich, Germany, 2008; ISBN 9783446409804.
22. Girard, S.; Alessi, A.; Richard, N.; Martin-Samos, L.; De Michele, V.; Giacomazzi, L.; Agnello, S.; Di Francesca, D.; Morana, A.; Winkler, B.; et al. Overview of radiation induced point defects in silica-based optical fibers. *Rev. Phys.* **2019**, *4*, 100032. [[CrossRef](#)]
23. Şen, M.; Aksüt, D.; Karaağaç, B. The effect of ionizing radiation on the mechanical properties of NBR elastomers reinforced by lignin. *Radiat. Phys. Chem.* **2020**, *168*, 108626. [[CrossRef](#)]
24. *ASTM D412-06a*; Vulcanized Rubber and Thermoplastic Elastomers–Tension. ASTM International: West Conshohocken, PA, USA, 2021.
25. *ASTM C20-00*; ASTM Standard Test Methods for Apparent Porosity, Water Absorption, Apparent Specific Gravity, and Bulk Density of Burned Refractory Brick and Shapes by Boiling Water. ASTM International: West Conshohocken, PA, USA, 2015.
26. Singh, V.P.; Badiger, N.M.; Kaewkhao, J. Radiation shielding competence of silicate and borate heavy metal oxide glasses: Comparative study. *J. Non Cryst. Solids* **2014**, *404*, 167–173. [[CrossRef](#)]
27. Singh, N.; Singh, K.J.; Singh, K.; Singh, H. Comparative study of lead borate and bismuth lead borate glass systems as gamma-radiation shielding materials. *Nucl. Instrum. Methods Phys. Res. Sect. B Beam Interact. Mater. Atoms* **2004**, *225*, 305–309. [[CrossRef](#)]
28. Bashter, I.I. Calculation of radiation attenuation coefficients for shielding concretes. *Ann. Nucl. Energy* **1997**, *24*, 1389–1401. [[CrossRef](#)]
29. Gaafar, I.; El-Shershaby, A.; Zeidan, I.; El-Ahll, L.S. Natural radioactivity and radiation hazard assessment of phosphate mining, Quseir-Safaga area, Central Eastern Desert, Egypt. *NRIAG J. Astron. Geophys.* **2016**, *5*, 160–172. [[CrossRef](#)]
30. Rammah, Y.S.; Sayyed, M.I.; Abohaswa, A.S.; Tekin, H.O. FTIR, electronic polarizability and shielding parameters of B<sub>2</sub>O<sub>3</sub> glasses doped with SnO<sub>2</sub>. *Appl. Phys. A Mater. Sci. Process.* **2018**, *124*, 650. [[CrossRef](#)]
31. Sayyed, M.I.; Qashou, S.I.; Khattari, Z.Y. Radiation shielding competence of newly developed TeO<sub>2</sub>-WO<sub>3</sub> glasses. *J. Alloys Compd.* **2017**, *696*, 632–638. [[CrossRef](#)]
32. Umar, S.A.; Halimah, M.K.; Chan, K.T.; Amirah, A.A.; Azlan, M.N.; Grema, L.U.; Hamza, A.M.; Ibrahim, G.G. Optical and structural properties of rice husk silicate incorporated borotellurite glasses doped with erbium oxide nanoparticles. *J. Mater. Sci. Mater. Electron.* **2019**, *30*, 18606–18616. [[CrossRef](#)]
33. Tijani, S.A.; Kamal, S.M.; Al-Hadeethi, Y.; Arib, M.; Hussein, M.A.; Wageh, S.; Dim, L.A. Radiation shielding properties of transparent erbium zinc tellurite glass system determined at medical diagnostic energies. *J. Alloys Compd.* **2018**, *741*, 293–299. [[CrossRef](#)]
34. Sathiyaraj, P.; Samuel, E.J.J.; Valeriano, C.C.S.; Kurudirek, M. Effective atomic number and buildup factor calculations for metal nano particle doped polymer gel. *Vacuum* **2017**, *143*, 138–149. [[CrossRef](#)]
35. Kavaz, E.; Yorgun, N.Y. Gamma ray buildup factors of lithium borate glasses doped with minerals. *J. Alloys Compd.* **2018**, *752*, 61–67. [[CrossRef](#)]
36. El-Kameesy, S.U.; Youssef, G.M.; El-Zaiat, S.Y.; Saudi, H.A.; Abd El-Kawy, F.S. Gamma Rays Attenuation Properties and the Associated Optical and Mechanical Behavior of Development (70-x) B<sub>2</sub>O<sub>3</sub>-10Al<sub>2</sub>O<sub>3</sub>-10Na<sub>2</sub>O-10ZnO-x PbO Glasses. *Silicon* **2018**, *10*, 1881–1886. [[CrossRef](#)]
37. Oto, B.; Gür, A.; Kavaz, E.; Çakır, T.; Yaltay, N. Determination of gamma and fast neutron shielding parameters of magnetite concretes. *Prog. Nucl. Energy* **2016**, *92*, 71–80. [[CrossRef](#)]
38. Harima, Y. An historical review and current status of buildup factor calculations and applications. *Radiat. Phys. Chem.* **1993**, *41*, 631–672. [[CrossRef](#)]

39. Kaplan, M.F. *Concrete Radiation Shielding: Nuclear Physics, Concrete Properties, Design and Construction*; Longman Scientific & Technical: Harlow, UK, 1989; ISBN 0470213388.
40. Singh, V.P.; Badiger, N.M. Gamma ray and neutron shielding properties of some alloy materials. *Ann. Nucl. Energy* **2014**, *64*, 301–310. [[CrossRef](#)]
41. ANSI/ANS-6.4.3; Gamma-Ray Attenuation Coefficients and Buildup Factors for Engineering Materials. American Nuclear Society: La Grange Park, IL, USA, 1991.
42. White, J.; De, S.K. *Rubber Technologist's Handbook*; Rapra Technology Ltd.: Shawbury, UK, 2001; ISBN 1859572626.
43. El-Fiki, S.; El Kameesy, S.U.; Nashar, D.E.; Abou-Leila, M.A.; El-Mansy, M.K.; Ahmed, M. Influence of Bismuth Contents on Mechanical and Gamma Ray Attenuation Properties of Silicone Rubber Composite. *Int. J. Adv. Res.* **2015**, *3*, 1035–1041.
44. Marković, G.; Marinović-Cincović, M.S.; Jovanović, V.; Samaržija-Jovanović, S.; Budinski-Simendić, J. Gamma irradiation aging of NBR/CSM rubber nanocomposites. *Compos. Part B Eng.* **2012**, *43*, 609–615. [[CrossRef](#)]
45. Elabbasy, M.T.; Abd El-Kader, M.F.H.; Ismail, A.M.; Menazea, A.A. Regulating the function of bismuth (III) oxide nanoparticles scattered in Chitosan/Poly (Vinyl Pyrrolidone) by laser ablation on electrical conductivity characterization and antimicrobial activity. *J. Mater. Res. Technol.* **2021**, *10*, 1348–1354. [[CrossRef](#)]
46. Silverstein, R.M.; Webster, F.X.; Kiemle, D.J. *Spectrometric Identification of Organic Compounds*, 7th ed.; John Wiley & Sons: New York, NY, USA, 2005; ISBN 0-471-39362-2.
47. Herzberg, G.; Crawford, B.L. Infrared and Raman Spectra of Polyatomic Molecules. *J. Phys. Chem.* **1946**. [[CrossRef](#)]
48. Smith, B. *Infrared Spectral Interpretation: A Systematic Approach*; CRC Press: Boca Raton, FL, USA, 2018.
49. Atef, S.; El-Nashar, D.E.; Ashour, A.H.; El-Fiki, S.; El-Kameesy, S.U.; Medhat, M. Effect of gamma irradiation and lead content on the physical and shielding properties of PVC/NBR polymer blends. *Polym. Bull.* **2020**, *77*, 5423–5438. [[CrossRef](#)]
50. Samir, A.; El-Nashar, D.E.; Ashour, A.H.; Medhat, M.; El-Kameesy, S.U. Polyvinyl chloride/styrene butadiene rubber polymeric blend filled with bismuth subcarbonate (BiO)<sub>2</sub>CO<sub>3</sub> as a shielding material for gamma rays. *Polym. Compos.* **2020**, *41*, 535–543. [[CrossRef](#)]
51. Ao, W.; Li, J.; Yang, H.; Zeng, X.; Ma, X. Mechanochemical synthesis of zinc oxide nanocrystalline. *Powder Technol.* **2006**, *168*, 148–151. [[CrossRef](#)]
52. Iqbal, T.; Sohaib, M. Synthesis of novel lanthanum-doped zinc oxide nanoparticles and their application for wastewater treatment. *Appl. Nanosci.* **2021**, *11*, 2599–2609. [[CrossRef](#)]
53. Utracki, L.A.; Wilkie, C.A. *Polymer Blends Handbook*; Kluwer Academic Publishers: Dordrecht, The Netherlands, 2014; ISBN 9789400760646.
54. Riaz, U.; Ashraf, S.M. Characterization of Polymer Blends with FTIR Spectroscopy. In *Characterization of Polymer Blends: Miscibility, Morphology and Interfaces*; Wiley-VCH Verlag GmbH & Co. KGaA: Weinheim, Germany, 2015; ISBN 9783527645602.
55. Singh, V.P.; Badiger, N.M. Investigation on radiation shielding parameters of ordinary, heavy and super heavy concretes. *Nucl. Technol. Radiat. Prot.* **2014**, *29*, 149–156. [[CrossRef](#)]
56. Berger, M.J.; Photon Cross Sections Database. NIST Standard Reference Database 8 (XGAM). 1998. Available online: <http://physics.nist.gov/PhysRefData/Xcom/Text/XCOM.html> (accessed on 11 June 2023).
57. Sayyed, M.I.; Lakshminarayana, G.; Kityk, I.V.; Mahdi, M.A. Evaluation of shielding parameters for heavy metal fluoride based tellurite-rich glasses for gamma ray shielding applications. *Radiat. Phys. Chem.* **2017**, *139*, 33–39. [[CrossRef](#)]
58. El Abd, A.; Mesbah, G.; Mohammed, N.M.A.; Ellithi, A. A simple Method for Determining the Effective Removal Cross Section for Fast Neutrons. *J. Radiat. Nucl. Appl.* **2017**, *2*, 53–58. [[CrossRef](#)]
59. Otaguro, H.; de Lima, L.F.C.P.; Parra, D.F.; Lugão, A.B.; Chinelatto, M.A.; Canevarolo, S.V. High-energy radiation forming chain scission and branching in polypropylene. *Radiat. Phys. Chem.* **2010**, *79*, 318–324. [[CrossRef](#)]
60. Khonakdar, H.A.; Jafari, S.H.; Wagenknecht, U.; Jehnichen, D. Effect of electron-irradiation on cross-link density and crystalline structure of low- and high-density polyethylene. *Radiat. Phys. Chem.* **2006**, *75*, 78–86. [[CrossRef](#)]

**Disclaimer/Publisher's Note:** The statements, opinions and data contained in all publications are solely those of the individual author(s) and contributor(s) and not of MDPI and/or the editor(s). MDPI and/or the editor(s) disclaim responsibility for any injury to people or property resulting from any ideas, methods, instructions or products referred to in the content.